Mirror contamination in space I: mirror modelling

J. M. Krijger[1], **R. Snel**[1], **G. van Harten**[2], **J. H. H. Rietjens**[1], **and I. Aben**[1]

[1]SRON Netherlands Institute for Space Research, Sorbonnelaan 2, 3584CA Utrecht, the Netherlands
[2]Leiden Observatory, Leiden University, Niels Bohrweg 2, 2333CA Leiden, the Netherlands

Correspondence to: J. M. Krijger (krijger@sron.nl)

Abstract. We present a comprehensive model that can be employed to describe and correct for degradation of (scan) mirrors and diffusers in satellite instruments that suffer from changing optical Ultraviolet to visible (UV–VIS) properties during their operational lifetime. As trend studies become more important, so does the importance of understanding and correcting for this degradation. This is the case not only with respect to the transmission of the optical components, but also with respect to wavelength, polarisation, or scan-angle effects. Our hypothesis is that mirrors in flight suffer from the deposition of a thin absorbing layer of contaminant, which slowly builds up over time. We describe this with the Mueller matrix formalism and Fresnel equations for thin multi-layer contamination films. Special care is taken to avoid the confusion often present in earlier publications concerning the Mueller matrix calculus with out-of-plane reflections. The method can be applied to any UV–VIS satellite instrument. We illustrate and verify our approach to the optical behaviour of the multiple scan mirrors of SCIAMACHY (onboard EN-VISAT).

1 Introduction

Almost all optical instruments in space suffer from transmission loss due to in-flight degradation of optical components and/or detectors. This transmission loss, especially at shorter Ultraviolet (UV) wavelengths, can, in the worst case, cause a nearly complete loss of detectable photons, and in lesser cases a strong decrease in the signal-to-noise ratio. Often this transmission loss is corrected by solar calibration, e.g. by using a diffuser to observe the (assumed stable) sun. However, instruments employing scan mirrors often observe their scientific targets under different angles than their (in-flight)

calibration sources. As more satellites spent longer times in orbit, it became clear that the transmission loss or degradation is dependent on the scan angle (of the scan mirror) (Krijger et al., 2005b; Tilstra et al., 2012). This has been referred to as the scan-angle-dependent degradation. This problem is becoming more pressing with the increasing number of long-term (climate) trend studies.

Our hypothesis is that both scan mirrors and surface diffusers suffer from a thin absorbing layer of contaminant, which slowly builds up over time. Many previous studies of such contaminant layers that form on mirrors and/or diffusers in space have been performed. However, despite their good quality, many authors decided not to publish in peer-reviewed scientific journals. Studies like e.g. the one by Stiegman et al. (1993) on diffusers, show some organic effluent present, but did not allow for the identification of the contaminant. Also, Chommeloux et al. (1998) showed the on-ground degradation as a result of UV or photon radiation, as did Georgiev and Butler (2007) or Fuqua et al. (2004). In-flight studies of contaminant are of course more difficult. Some studies are collected in an extensive database, which has recently been made available to the general public (Green, 2001). In summary, most of the early satellites suffered from degradation caused by outgassing. However, the exact identity of the contaminant causing the Ultraviolet to visible (UV–VIS) degradation remained unclear. McMullin et al. (2002) studied the degradation of SOHO/SEM, and found that they could explain the degradation with a thin layer of carbon forming on the forward aluminium filter. The exact source of the contaminant is unknown, but is suspected to be outgassing of the satellite itself. Schläppi et al. (2010) attempted in situ mass spectrometry with ROSETTA to measure the constituents of their contamination, and found the main contaminants to be water. In addition, organics from the spacecraft structure,

electronics and insulations were identified. Water was also found in SCIAMACHY, where it was deposited onto the cold detectors (Lichtenberg et al., 2006). In fact, Earth-observing satellites suffer from degradation, both in throughput and in the polarisation and/or scan-angle dependence, such as GOME (Krijger et al., 2005a; Slijkhuis et al., 2006), MODIS (Xiong et al., 2003; Xiong and Barnes, 2006; Meister and Franz, 2011), SeaWiFs (Eplee et al., 2007), VIIRS (Lei et al., 2012), MERIS (Delwart, 2010), SCIAMACHY (Bramstedt et al., 2009)[1], and the two GOME-2 (Lang, 2012) instruments currently in orbit. Most provide an empirical degradation correction for the data users.

Thin layer deposits on mirrors and diffusers have been modelled before (e.g. most recently by Lei et al., 2012); however, these earlier attempts focus only on transmission loss, and often do not take scan-angle dependence into account, and none consider polarisation. These, however, need to be considered for a proper description of in-flight behaviour. This can be done by employing the Mueller matrix formalism and Fresnel equations. The application of Mueller matrix calculation in combination with the Fresnel equations requires special care due to their different mathematical descriptions of polarised light, especially in the case of out-of-plane reflections. However, there are many ambiguities in often not well-defined absolute polarisation frames, in the direction or handedness in the often ignored circular polarisation, in naming conventions, or in the application of signs with respect to frame changes, which often lead to much confusion. Therefore, in this paper, we go for the first time[2] into full detail, and present a consistent, well-defined approach to Mueller matrix calculation in combination with Fresnel equations, using detailed illustrations and descriptions to describe the mathematics and frames. We will show that this approach is in full agreement with verification measurements, and is generally applicable.

As the first paper in a planned series on in-flight mirror contamination, this initial paper focuses on the mathematical modelling of the mirror with possible contaminants. Further application to in-flight measurements and how to derive optical properties of in-flight contaminations will be presented in a follow-up paper.

This study was initiated to investigate the wavelength and scan-angle-dependent degradation as observed by SCIAMACHY, onboard ENVISAT (Gottwald and Bovensmann, 2011), which affects long-term data records. The optical behaviour of the scan mirror of SCIAMACHY has been simulated based on this model, and was compared with measurements during on-ground calibration and dedicated laboratory measurements, which show that the model performs very satisfactorily under those early on-ground conditions. Analyses of in-flight SCIAMACHY contaminations and its behaviour over time will also be presented in a follow-up paper.

---

[1]Data at http://www.iup.uni-bremen.de/sciamachy/mfactors/.

[2]To the authors' knowledge.

The great value of this model is that it is generally applicable and can easily be applied to all satellites, employing (scan) mirrors or other reflecting optics suffering from degradation due to contamination. The model, once applied, can provide detailed scan-angle and wavelength behaviour as a function of time, allowing for accurate correction, which is needed for precise (trend) analyses.

In Sect. 2, we describe a model for a scan mirror and a surface diffuser. In Sect. 3, we shortly describe SCIAMACHY, important for our verification. This verification using on-ground measurements is described in Sect. 4. A general discussion follows. Finally, we will draw conclusions on the model with an outlook to its application.

2   Model

2.1   Mueller calculus

In order to model the scan-angle-dependent throughput of mirrors, we employ the well-known Stokes and Mueller calculus (Azzam and Bashara, 1987; Hecht, 1987). The incoming (partly) polarised light is characterised by a Stokes vector $\boldsymbol{I}$

$$\boldsymbol{I} = \begin{pmatrix} I \\ Q \\ U \\ V \end{pmatrix}, \tag{1}$$

Here, I is the intensity, Q and U describe the two-dimensional state of linear polarisation, and V represents circular polarisation.

Any description of polarisation requires an exact reference frame definition. In this paper, we use the same reference frame and conventions as Hecht (1987). This means that when looking along the direction in which the light is travelling, positive U is found by rotating 45° anticlockwise from Q, while positive V is defined when the E vector is rotating clockwise, as shown in Fig. 1. Note that the rotation and direction of the E vector is defined in a fixed reference frame or plane. Many other frame definitions are in use; however, these will require different Mueller matrices than those used in this text.

The Stokes vector $\boldsymbol{I}$ is often split into a total signal part and a polarisation vector,

$$\boldsymbol{I} = I_0 \cdot \begin{pmatrix} 1 \\ q \\ u \\ v \end{pmatrix}, \tag{2}$$

with q, u, and v the fractional polarisation Q, U, and V with respect to the total signal, I_0.

Any detected signal S depends on the received polarised light $\boldsymbol{I}$ and the polarisation sensitivity of the instrument $\boldsymbol{\mu}$,

$$S = \boldsymbol{\mu} \cdot \boldsymbol{I}, \tag{3}$$
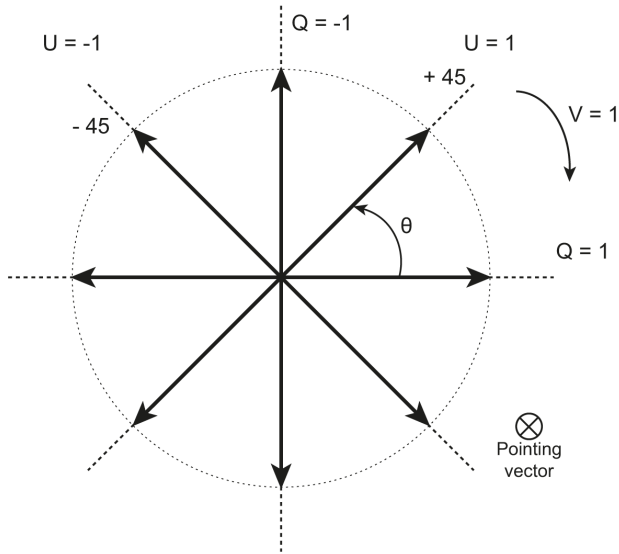
Figure 1. Stokes vector frame definition used in the paper. Pointing vector is perpendicular and into the paper (following the light).

with

$$\boldsymbol{\mu} = M_1 \cdot (1, \mu_2, \mu_3, \mu_4), \tag{4}$$

with M_1 the absolute radiance sensitivity of the instrument and μ_x the normalised polarisation sensitivity of q, u, and v of the instrument, respectively.

Any optical element that modifies the polarised light, such as retarders, polarisers, and mirrors, can be described as a 4×4 transformation matrix $\mathbf{M}$ (known as the Mueller matrix):

$$S = \boldsymbol{\mu} \cdot \mathbf{M} \cdot \boldsymbol{I}. \tag{5}$$

For polarisation-insensitive detectors, the first row of $\mathbf{M}$ is often considered equivalent to $\boldsymbol{\mu}$, thus removing the need for $\boldsymbol{\mu}$. However, here we consider a possible polarisation-sensitive instrument, and choose to employ $\boldsymbol{\mu}$ explicitly.

Multiple elements encountered by the light can be described by multiplying consecutive Mueller matrices:

$$S = \boldsymbol{\mu} \cdot \mathbf{M}_n \ldots \mathbf{M}_3 \mathbf{M}_2 \mathbf{M}_1 \cdot \boldsymbol{I}. \tag{6}$$

Note that, for Mueller matrix calculations, the first encountered element by the light is the one farthest right in the formula. Matrix multiplication is not commutative, so order is important.

It is always important to define the reference frame both at the detector and at the source, and to keep track of the frame at different positions between source and detector, since a frame rotation might be needed between two optical components when out-of-plane reflections happen. In reflections, the p and s directions are often used. The p polarisation (p from "parallel") is the polarisation in the plane of reflection or incidence, while s polarisation (s from "senkrecht", German for perpendicular) is perpendicular to this plane (see
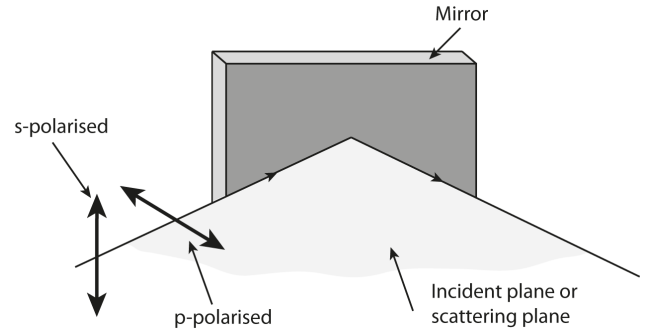

Figure 2. s and p polarisation direction definitions for a reflection.

Fig. 2). The p and s frame can be, and often is, coupled to a Stokes frame in the case of a single reflection, with $S \equiv Q = 1$ and $P \equiv Q = -1$. However, this is a choice and can be different, as long as the Stokes frame is rotated before and after a reflection to the p and s frame (see Sect. 2.5 for more details on frame rotations). For example, the mirror in Fig. 2 would have to be rotated 90° in order to match the frame from Fig. 1 with $S \equiv Q = 1$.

2.2 Mirror model

The generic Mueller matrix for a mirror, defined in the reference frame of Fig. 1, with the angle of incidence of the light given by i_{mir} and the plane of reflection perpendicular to the $Q = 1$ direction, is given by Azzam and Bashara (1987):

$$\mathbf{M}_{\mathrm{mir}}(\phi_{\mathrm{mir}}) = \begin{pmatrix} \frac{1}{2}(r_s^2 + r_p^2) & \frac{1}{2}(r_s^2 - r_p^2) & 0 & 0 \\ \frac{1}{2}(r_s^2 - r_p^2) & \frac{1}{2}(r_s^2 + r_p^2) & 0 & 0 \\ 0 & 0 & |r_p||r_s|\cos(\Delta) & |r_p||r_s|\sin(\Delta) \\ 0 & 0 & -|r_p||r_s|\sin(\Delta) & |r_p||r_s|\cos(\Delta) \end{pmatrix}, \tag{7}$$

where the complex reflection coefficients r_p and r_s for s- and p-polarised light are given by the Fresnel equations

$$r_p = \frac{n_2 \cos(\phi_{\mathrm{mir}}) - n_1 \sqrt{1 - \left(\frac{n_1}{n_2} \sin(\phi_{\mathrm{mir}})\right)^2}}{n_2 \cos(\phi_{\mathrm{mir}}) + n_1 \sqrt{1 - \left(\frac{n_1}{n_2} \sin(\phi_{\mathrm{mir}})\right)^2}}, \tag{8}$$

$$r_s = \frac{n_1 \cos(\phi_{\mathrm{mir}}) - n_2 \sqrt{1 - \left(\frac{n_1}{n_2} \sin(\phi_{\mathrm{mir}})\right)^2}}{n_1 \cos(\phi_{\mathrm{mir}}) + n_2 \sqrt{1 - \left(\frac{n_1}{n_2} \sin(\phi_{\mathrm{mir}})\right)^2}}. \tag{9}$$

The complex indices of refraction of the mirror material and ambient medium are denoted by n_2 and n_1. Note that $n = n_{\mathrm{r}} - ik$, with $k \geq 0$, with n_{r} the real part and k the imaginary part. This makes k a damping factor, which describes the absorption of light by metals (see van Harten et al., 2009). Note that the s and p directions are given here according to the conventional definition, with p in the plane of reflection

and s perpendicular to this plane. The phase jump Δ in this coordinate frame is defined as

$$\Delta \;=\; \arg(r_p) - \arg(r_s). \tag{10}$$

On a side note: a perfect reflection is described by

$$\mathbf{M}_{\text{perfect reflection}} = \begin{pmatrix} 1 & 0 & 0 & 0 \\ 0 & 1 & 0 & 0 \\ 0 & 0 & -1 & 0 \\ 0 & 0 & 0 & -1 \end{pmatrix}. \tag{11}$$

The reflection Mueller matrix correctly describes that the signs of U and V flip. This is a direct consequence of the fact that the Stokes frame is defined for an observer looking along the beam, so upon reflection, the definitions of left and right are swapped. This sign change of U and V can be achieved mathematically by changing the signs in the lower-right quadrant of the mirror Mueller matrix (see e.g. Keller, 2002), or as was done here, by the definition of Δ with r_p and r_s, which cause a 180° phase difference for a perfect reflection.

2.3 Diffuser model

The mirror model can also be employed to describe the behaviour of a surface diffuser. The roughened surface contains many irregularities (or facets) which cause light to be reflected in various directions, thus decreasing the transmission in the direction of the instrument. The assumption here is made that for polarisation behaviour, the diffuser can be considered to be a large number of small mirror facets. Only those facets contribute to the signal which are oriented such that they cause specular reflection of the light into the direction of the instrument (see Fig. 3). The geometry thus dictates the relative polarisation behaviour, while the unpolarised reflectivity is only a function of the angular distribution of the facets of the diffuser and the orientation of the diffuser in the light path. The Mueller matrix for a surface diffuser is then given by

$$\mathbf{M}_{\text{dif}}(\phi_{\text{in}}, \phi_{\text{out}}) = M_1^{\text{dif}}(\phi_{\text{in}}, \phi_{\text{out}}) \cdot \mathbf{M}_{\text{mir}}(\phi_{\text{dif}}), \tag{12}$$

with the scalar M_1^{dif} the diffuser sensitivity and

$$\phi_{\text{dif}} = \frac{1}{2}(\phi_{\text{in}} + \phi_{\text{out}}), \tag{13}$$

with ϕ_{in} and ϕ_{out} both positive angles with respect to the normal, and $\mathbf{M}_{\text{mir}}$ as in Eq. 7. Figure 3 shows the various angles.

2.4 Contamination

Our hypothesis is that degrading mirrors and diffusers degrade through deposition of thin absorbing layers of contaminant, which change over time. The model was thus extended to allow up to two layers with a specified thickness and refractive index (Azzam and Bashara, 1987; Born and Wolf,
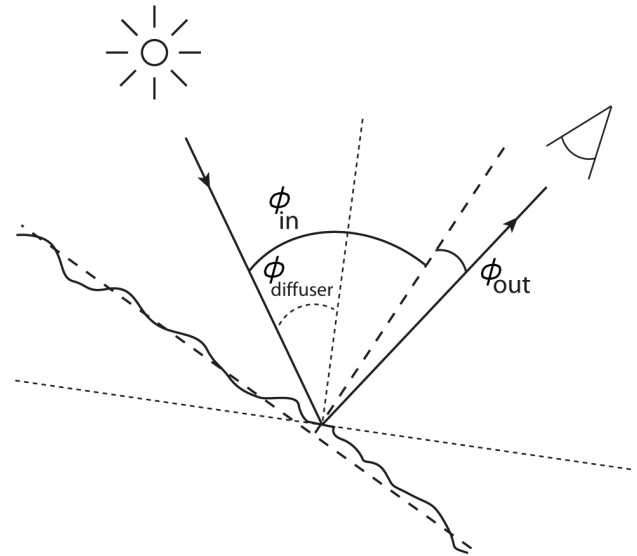
Figure 3. Angle definitions used in the mirror model for diffuser geometries. Solid curves with arrows indicate the light beam of interest with direction; long dashed curves indicate the macro-scale surface of the diffuser and its normal. Short dashed curves indicate the extrapolated surface and normal of the facet that causes the specular reflection of the light beam of interest. The various random (micro-scale) facets of the diffuser are indicated by the wiggly solid curve. Only facets oriented such that they cause specular reflection in the direction of the instrument contribute to the signal, dictating relative polarisation behaviour. Unpolarised reflectivity is only a function of the angular distribution of the facets of the diffuser, and the orientation of the diffuser in the light path.

1999). The change to the model, as presented in Sect. 2.2, is only in the equations for the reflection coefficients r_s and r_p, combined here as an implied s- and p-specific reflection coefficient R_t. We employ a capital R for combined multi-layer intensity reflections at a certain interface, which incorporates the direct reflection at the interface and all (multiple) reflection from subsequent layers. Note that this is a different approach from that described in van Harten et al. (2009), as we include each extra layer explicitly. The total reflection coefficient for the bulk or substrate (subscript 4) with refractive index n_4, the second layer (subscript 3) with refractive index n_3, the first layer (subscript 2) with refractive index n_2, and the ambient medium (subscript 1) with refractive index n_1 combined, is given by (see also Fig. 4 for a graphical explanation, and Azzam and Bashara, 1987)

$$R_t \;=\; \frac{r_{12} + R_{23}e^{(-2i\delta_2)}}{1 + r_{12}R_{23}e^{(-2i\delta_2)}}, \tag{14}$$

where r_{jk} are the r_s and r_p reflection coefficients between media with subscripts j and k, as given by Eqs. (8) and (9), and by

$$\delta_2 \;=\; 2\pi \frac{d_2}{\lambda} n_2 \cos(\phi_2), \tag{15}$$
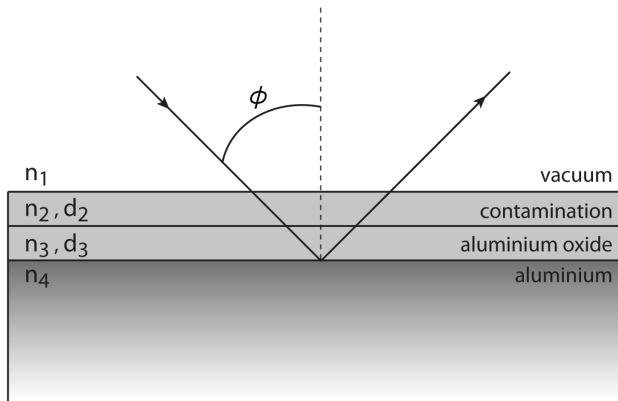
Figure 4. Layers and angle definitions used in the mirror model with thickness (d_i) and complex refractive index (n_i). Left: annotation for the general case; right: materials for SCIAMACHY application.

$$\cos(\phi_2) = \sqrt{1 - \left(\frac{n_1}{n_2}\sin(\phi_1)\right)^2}, \tag{16}$$

$$R_{23} = \frac{r_{23} + r_{34}e^{(-2i\delta_3)}}{1 + r_{23}r_{34}e^{(-2i\delta_3)}}. \tag{17}$$

$$\delta_3 = 2\pi\frac{d_3}{\lambda}n_3\cos(\phi_3), \tag{18}$$

$$\cos(\phi_3) = \sqrt{1 - \left(\frac{n_2}{n_3}\sin(\phi_2)\right)^2}$$
$$= \sqrt{1 - \left(\frac{n_1}{n_3}\sin(\phi_1)\right)^2}, \tag{19}$$

with ϕ_x the angle of incidence in medium x (only ϕ_1 is needed; the others can be derived as shown), λ the wavelength of the light, and d_2 and d_3 the layer thicknesses of the layers closest to the ambient medium and the substrate, respectively.

To expand the model to any desired number of layers, the total reflectance R_t at the top interface of a multi-layer system can be calculated by determining the combined (multi-layer) reflectance at the interface between the ambient medium (subscript 1) and the first layer (index 2), R_{12}, as done in Eq. (14). However, Eq. (17) must be expanded to the general case, where the combined (multi-layer) reflectance at the interface between layer or medium i and layer j (with $j = i + 1$), namely $R_{i,j}$, is given by

$$R_{i,j} = \frac{r_{i,j} + R_{j,j+1}e^{(-2i\delta_j)}}{1 + r_{i,j}R_{j,j+1}e^{(-2i\delta_j)}}, \tag{20}$$

with

$$\delta_j = 2\pi\frac{d_j}{\lambda}n_j\cos(\phi_j), \tag{21}$$

$$\cos(\phi_j) = \sqrt{1 - \left(\frac{n_i}{n_j}\sin(\phi_i)\right)^2}. \tag{22}$$

R_{12} can thus be calculated by successively employing Eq. (20)–(22) for incrementing layers i and j until an effectively infinite layer $n + 1$ (where $R_{n,n+1} = r_{n,n+1}$, as in Eq. 17) or the desired accuracy is reached.

2.5 Multiple mirrors

Some instruments, such as SCIAMACHY, employ multiple scan mirrors. As a result, both polarisation and throughput change as a function of the viewing angle of each mirror. The modelling of the reflection from multiple mirrors may require the use of rotation matrices. Especially in cases where the planes of two successive reflections are not parallel, a rotation of the reference frame is needed in order to align the $Q = 1$ direction of the reference frame with the s direction corresponding to the plane of reflection. The rotation matrix over an arbitrary angle γ is given by

$$\mathbf{R}(\gamma) = \begin{pmatrix} 1 & 0 & 0 & 0 \\ 0 & \cos(2\gamma) & -\sin(2\gamma) & 0 \\ 0 & \sin(2\gamma) & \cos(2\gamma) & 0 \\ 0 & 0 & 0 & 1 \end{pmatrix}. \tag{23}$$

Using this Mueller matrix with $\gamma = 45°$ changes $Q = 1$ into $U = 1$. In order to add an optical element with Mueller matrix $\mathbf{M}$ placed at an angle γ, one has to rotate the element mathematically in line as follows, to get it to align with our frame:

$$\mathbf{M}_{\text{rot}} = \mathbf{R}(\gamma) \cdot \mathbf{M} \cdot \mathbf{R}(-\gamma). \tag{24}$$

For a mirror, where the reflection flips the coordinates, the back transformation should hence also be mirrored (Keller, 2002), resulting in

$$\mathbf{M}_{\text{rot}} = \mathbf{R}(-\gamma) \cdot \mathbf{M} \cdot \mathbf{R}(-\gamma). \tag{25}$$

For clarity, note that all rotation signs can be swapped as long as they are then also changed in the rotation matrix. Sometimes both definitions are used in the same book, e.g. in Azzam and Bashara (1987). Note that for polarisation, two positive rotations do not equal two negative rotations, due to the handedness of polarisation.

Combining the two mirrors can then be written as

$$\begin{aligned} \mathbf{M}_{\text{mir}}(\phi_{\text{mir1}}, \phi_{\text{mir2}}) = {} & \\ & \mathbf{R}(-\gamma_{\text{mir2}}) \cdot \mathbf{M}(\phi_{\text{mir2}}) \cdot \mathbf{R}(-\gamma_{\text{mir2}}) \\ & \cdot \mathbf{R}(-\gamma_{\text{mir1}}) \cdot \mathbf{M}(\phi_{\text{mir1}}) \cdot \mathbf{R}(-\gamma_{\text{mir1}}). \end{aligned} \tag{26}$$

Each rotation is with respect to the Stokes frame of the light incident on the optical element. This allows changing from e.g. an external frame to an instrument frame and vice versa by adding the appropriate rotation matrix. When employing two mirrors, the angle of incidence on the second mirror depends on the angles at which the mirrors are rotated with respect to each other. An example of modelling two mirrors applied to the case of SCIAMACHY will be shown in the next section.

3 SCIAMACHY

The SCIAMACHY (Gottwald et al., 2006) calibration concept (Noël et al., 2003) builds on a combination of on-ground and in-flight calibration measurements. The on-ground calibration measurements were split up into ambient measurements comprising the scanner unit only, and thermal vacuum (TV) measurements using the entire instrument. Viewing angle dependence for the on-ground calibration data is derived from the ambient measurements, while the remainder of the calibration information is derived from the TV measurements. For in-flight conditions, the combination of ambient and TV data is essential.

Unforeseen instrumental polarisation behaviour, most likely caused by thermally induced stress birefringence of one of the optical components in the instrument (Snel, 2000), required the initial calibration approach to be extended, with additional on-ground polarisation characterisation of the instrument.

Shortly after launch, discrepancies between the observed and expected signals were observed, and subsequently significantly reduced by means of ad hoc sign changes of selected polarisation calibration parameters. This solution was considered acceptable for the time being, and worked well for nadir viewing geometry, but needed additional workarounds for limb geometry. Here however we will now employ a more fundamental approach. Our method is consistent in both nadir and limb, as we now describe the various mirrors in the same frame.

3.1 SCIAMACHY mirrors

Aluminium mirrors are known to induce instrumental polarisation when used at non-normal incidence (e.g. Thiessen and Broglia, 1959). Such mirrors however are often used in telescope mirrors, as onboard SCIAMACHY. This phenomenon is caused by differential reflection between polarisation in the plane of incidence and polarisation perpendicular to it, as described by the Fresnel equations. The amount of polarisation depends on the mirror material, angle of incidence, and wavelength. For instance, reflection off an aluminium mirror at 45° turns unpolarised visible light into 3 to 4% polarisation perpendicular to the plane of incidence (van Harten et al., 2009).

It has been shown that these polarisation properties can not be described using the Fresnel equations for bare aluminium (Burge and Bennett, 1964). Attempts to fit measured instrumental polarisation to an aluminium model lead to unrealistic pseudo-indices of refraction (Sankarasubramanian et al., 1999; Joos et al., 2008).

Indeed, this bare aluminium model is incomplete, since the instant an aluminium mirror is exposed to air, an aluminium oxide layer a few nanometers thick starts growing on its surface. This phenomenon, as explained theoretically by Mott (1939), was measured using microscopy and spectroscopy by Jeurgens et al. (2002). Mueller matrix ellipsometry by van Harten et al. (2009) showed that the mirror polarisation can be described by a $\sim 4.12 \pm 0.08$ nm aluminium oxide layer on top of bulk aluminium, where the layer grows asymptotically to the final thickness within the first ~ 10 days. This is also needed to describe the aluminium mirrors in SCIAMACHY adequately.

3.2 SCIAMACHY geometry

The SCIAMACHY scanner (Fig. 5) consists of two mechanisms, each containing a mirror with a diffuser on the back. The elevation scan mirror (ESM) is needed for all measurement modes and contains the main diffuser. The azimuth scan mirror (ASM) is only used in limb measurement mode, including the Sun over ESM diffuser mode. The ESM and ASM can be set at any angle.

SCIAMACHY has a geometry where detector and both mirrors are in the same plane, but with a perpendicular rotation axis (see Fig. 5). Let α_x be the rotation of mirror x around its axis, with 45° mirror rotation resulting in the light being reflected at 90°. For the ESM (employed for both the nadir and limb scans), the angle of incidence towards the detector is equal to the rotation of the ESM on its axis:

$$\phi_{\mathrm{ESM}} = \alpha_{\mathrm{ESM}}. \qquad (27)$$

When choosing the Stokes reference frames optimally (namely $S \equiv Q = 1$ for the ESM), the nadir case is very simple:

$$\mathbf{M}_{\mathrm{nadir}}^{\mathrm{opt}} = \mathbf{M}(\phi_{\mathrm{ESM}}). \qquad (28)$$

For limb observations, the situation is a bit more complicated, because one has to account for the different orientation of the planes of reflection of the ESM and ASM with respect to the Stokes reference frames of the incoming and outgoing light. The rotation angle between the plane of reflection of the ESM and the ASM is given by

$$\gamma_{\mathrm{ASM} \to \mathrm{ESM}} = \pi/2 + \arcsin(\cot(\phi_{\mathrm{mir1}}) \cdot \tan(2\phi_{\mathrm{mir2}})). \qquad (29)$$

Also, the ASM must be placed at a very specific angle in order to reflect the light onto the ESM and then the detector/instrument slit. The required angle of incidence on the
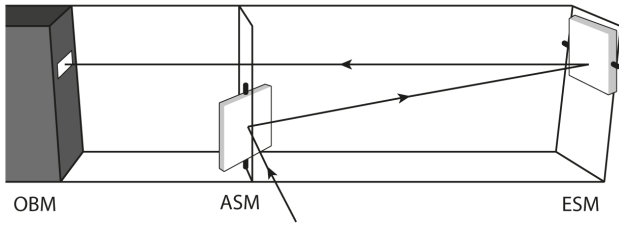
Figure 5. Schematic view of SCIAMACHY multiple mirror setup in limb observation mode. On the left side, the Optical Bench Module (OBM) and entrance slit. On the right side, the ESM, which if rotated to a 45° angle will reflect light (curve with arrow head) coming from below (nadir) directly into the slit. In the middle, the ASM, which reflects the (limb) light coming from the front and slightly below onto the ESM. Both mirrors have a bead-blasted aluminium surface diffuser on their back side (not shown here).

ASM can be calculated using

$$\phi_{\mathrm{ASM}} = \arccos(\cos(\alpha_{\mathrm{ASM}}) \cdot \cos(2\alpha_{\mathrm{ESM}})). \quad (30)$$

The total Mueller matrix for limb observations is then given by

$$\begin{aligned}
\mathbf{M}_{\mathrm{limb}}^{\mathrm{opt}} = {} & \mathbf{M}(\phi_{\mathrm{ESM}}) \cdot \mathbf{R}(-\gamma_{\mathrm{ASM}\to\mathrm{ESM}}) \\
& \cdot \mathbf{M}(\phi_{\mathrm{ASM}}) \cdot \mathbf{R}(-\gamma_{\mathrm{ASM}\to\mathrm{ESM}}).
\end{aligned} \quad (31)$$

However, for historical reasons, the $Q = 1$ direction was chosen perpendicular to the entrance slit of SCIAMACHY (see Fig. 5), i.e. parallel to the scattering plane of the ESM, or 90° compared to the simple case. This requires several rotations, resulting in a Mueller matrix for nadir observations:

$$\mathbf{M}_{\mathrm{nadir}}^{\mathrm{hist}} = \mathbf{R}(-\gamma_{\mathrm{ESM}}) \cdot \mathbf{M}(\phi_{\mathrm{ESM}}) \cdot \mathbf{R}(-\gamma_{\mathrm{ESM}}), \quad (32)$$

with $\gamma_{\mathrm{ESM}} = 90°$.

The total Mueller matrix for limb observations derived by frame rotating for each mirror element is then given by

$$\begin{aligned}
\mathbf{M}_{\mathrm{limb}}^{\mathrm{hist}} = {} & \mathbf{R}(-\gamma_{\mathrm{ESM}}) \cdot \mathbf{M}(\phi_{\mathrm{ESM}}) \cdot \mathbf{R}(-\gamma_{\mathrm{ESM}}) \\
& \cdot \mathbf{R}(-\gamma_{\mathrm{ESM}}) \cdot \mathbf{R}(-\gamma_{\mathrm{ASM}\to\mathrm{ESM}}) \cdot \mathbf{M}(\phi_{\mathrm{ASM}}) \\
& \cdot \mathbf{R}(-\gamma_{\mathrm{ASM}\to\mathrm{ESM}}) \cdot \mathbf{R}(-\gamma_{\mathrm{ESM}}).
\end{aligned} \quad (33)$$

As rotations are commutative, and two 90° rotations equal a full rotation for polarisation, this equation can be simplified here to

$$\begin{aligned}
\mathbf{M}_{\mathrm{limb}}^{\mathrm{hist}} = {} & \mathbf{R}(-\gamma_{\mathrm{ESM}}) \cdot \mathbf{M}(\phi_{\mathrm{ESM}}) \cdot \mathbf{R}(-\gamma_{\mathrm{ESM}}) \\
& \cdot \mathbf{R}(-\gamma_{\mathrm{ASM}}) \cdot \mathbf{M}(\phi_{\mathrm{ASM}}) \cdot \mathbf{R}(-\gamma_{\mathrm{ASM}}),
\end{aligned} \quad (34)$$

with

$$\gamma_{\mathrm{ASM}} = \arcsin(\cot(\phi_{\mathrm{mir1}}) \cdot \tan(2\phi_{\mathrm{mir2}})). \quad (35)$$

Finally, we emphasise that these formulas will change if different Stokes reference frames are used, but the approach remains the same.

4 Verification

Combining Mueller matrix formalism with the Fresnel equations requires, especially in the case of out-of-plane reflections, a precise definition and bookkeeping of mathematical signs and conventions. In particular, this applies to the absolute polarisation frame, to the rotations between frames before and after reflection, to the handedness of circularly polarised light, and to the implementation in the form of an algorithm.

Hence, it is of the utmost importance to verify Mueller matrix calculations. In this section, we apply our model to SCIAMACHY on-ground measurements of the diffuser and scan mirrors. We show that all data can be explained well by using Mueller matrix calculations in combination with the Fresnel equations, confirming the correct use of these tools.

4.1 Refractive index

In the section below, we compare model calculations with older on-ground measurements performed on aluminium mirrors during SCIAMACHY calibration. As mentioned, these aluminium mirrors were not vacuum protected, and will thus have a thin layer of aluminium oxide on them. In order to describe these mirrors, the refractive index of aluminium and aluminium oxide is needed for the wavelength range of interest (here 300–2400 nm). However, there are several conflicting aluminium refractive indices available in the literature, namely the direct measurements found in Haynes (2013) and Palik (1985) and the Kramers–Kronig-derived values of Rakic (1995). While the differences in the refractive index can be several percent, the difference in specific applications is much harder to quantify. Our verification results improved very slightly when employing the indices of Rakic (1995), and hence the choice was made to employ these indices.

To the best of our knowledge, in the literature there is no complete information on the refractive index of amorphous aluminium oxide in the 0.2–2.4 µm wavelength range.

However, the work of Edlou et al. (1993) can be extrapolated to the desired wavelength range by using the Cauchy dispersion equation

$$n(\lambda) = A + B\lambda^{-2} + C\lambda^{-4}. \quad (36)$$

We employ the values found by Edlou et al. (1993) of 1.63, 2.25×10^3 nm^2, and 20.16×10^7 nm^4 for A, B and C, respectively. The two different methods produce the same refractive indices for aluminium oxide within uncertainties. The latter option was employed for its ability to interpolate accurately to desired wavelengths.

4.2 Mirror model verification

First we compared the mirror model with the measurements of van Harten et al. (2009). Shown in Fig. 6 is the comparison at 600 nm, using a refractive index for the aluminium
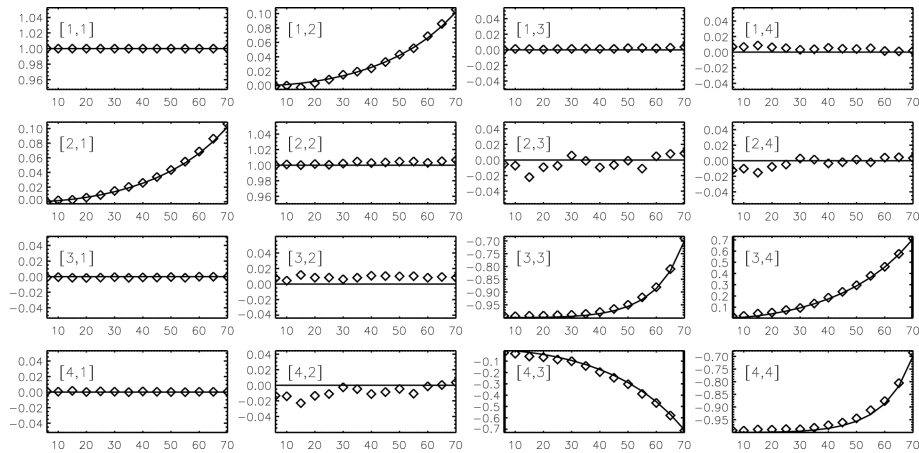
Figure 6. Normalised Mueller matrix of reflection off a real aluminium mirror with an aluminium oxide layer of measured 4.1 nm on top of it at 600 nm. Measurements by van Harten et al. (2009) (diamonds) and our model (lines).

of $1.262 - i7.186$ and a refractive index for the aluminium oxide, calculated by Eq. (36), of $1.637 - i0.000$ at the measured wavelength of 600 nm, for the different Mueller matrix components. The normalised, to the top-left element, measurements are assumed to be accurate within 0.02. The first-column components, the instrumental polarisation sensitivity here, has residuals smaller than 0.003, and are thus in almost perfect agreement. The diagonal components, indicating the transmission of polarisation, have residuals smaller than 0.01. Other (polarisation cross-talk) residuals remain below 0.02, but here the measurements might have suffered from limited calibration accuracy (for more discussion on the measurements, see van Harten et al., 2009). In summary, the residuals between measurement and model are within the measurement accuracy, hence the measurement data and model are in excellent agreement.

For another verification, we turned to SCIAMACHY. During on-ground calibration of the SCIAMACHY aluminium scan mirrors, reflectivity was measured with different polarisation orientations of the incoming light, with both single and multiple mirrors.

We show the most complicated situation first, with multiple mirrors where multiple orientations of linear polarisation ($Q = 1$, $Q = -1$, $U = 1$, and $U = -1$ with respect to the SCIAMACHY reference frame) were reflected on the whole scanner unit. The reflected light was then analysed by employing linear polarisation filters (either $Q = 1$ or $Q = -1$). Shown in Fig. 7 are both measurement and model simulations under the SCIAMACHY reference viewing angles ($\phi_{\mathrm{ESM}} = 12.7°$ and $\phi_{\mathrm{ASM}} = 45°$) for the various combinations of offered and measured polarisation directions. The original estimated errors bars are shown; however, already during the measurements, it was clear these were too optimistic (Dobber, 1999). As can be seen, the measurements originally differed several standard deviations from a simple clean mirror model employing the literature value for the

refractive index of aluminium. Including a 4.12 nm layer of aluminium oxide (van Harten et al., 2009) improves the comparison significantly; however, for the shortest wavelength, an additional contamination was needed. A correction by increasing the thickness of the aluminium oxide to 9 nm (not shown) showed improvement, but did not show the correct wavelength behaviour, and was rejected. Further investigation showed that employing 0.4 nm of light oil contamination on the surface of the mirrors would be consistent in order to model the measurements correctly.

The light oil optical properties were taken from Barbaro et al. (1991). Such a small contamination of 0.4 nm on the mirror was within the molecular cleanliness control requirements (van Roermund, 1996) during on-ground measurements. Of course, the exact kind of oil or even the kind of contaminant is unknown; however, the assumption of light oil contamination is not unreasonable. As both mirrors were kept under similar conditions, we assume a similar contamination of oil on both.

The good agreement between measurements and model clearly shows that the mirror model works very well, and that the inclusion of aluminium oxide and oil contamination is necessary for explaining the measurement results. Since an error or sign change in one of the rotation angles used in the calculation will result in completely different polarisation sensitivities (not shown here), Fig. 7 confirms that the correct signs and rotation angles are employed. The use of the optical properties of light oil, while the true contaminant source and its polarisation properties are as yet unknown, could be the reason for the differences at the shortest wavelengths. However, more likely the measurements have larger uncertainties than originally stated.

The single mirror measurements are less sensitive to contaminations, and are thus less useful for verification, but we show them here for completeness in Fig. 8. Again, a 4.1 nm aluminium oxide and 0.4 nm light oil contamination were
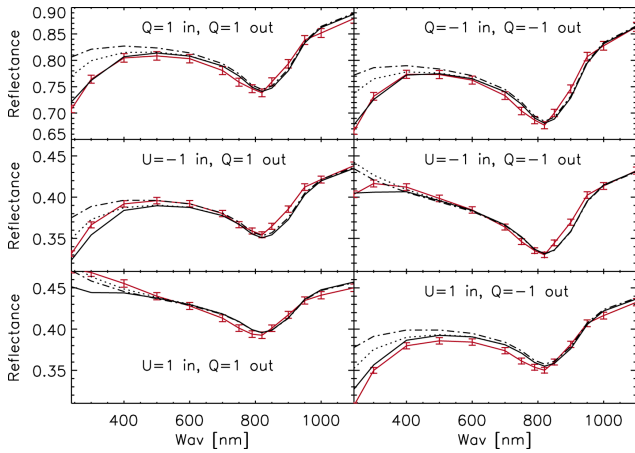
Figure 7. SCIAMACHY scan mirror reflectance for different polarisation states of the incident light ($Q = 1$, $Q = -1$, $U = 1$, and $U = -1$ with respect to the SCIAMACHY reference frame) and different orientation of the analysers ($Q = 1$ and $Q = -1$), as indicated in the subplots. The measurement results with error bars obtained during on-ground calibration are shown in red, while the model calculations are represented by the black solid curve. The model calculation includes an aluminium mirror with 4.1 nm aluminium oxide and 0.4 nm light oil contamination, and angles of incidence $\phi_{\mathrm{ESM}} = 12.7°$ and $\phi_{\mathrm{ASM}} = 45°$. Dash–dotted curves indicate clean aluminium, and dotted curves aluminium with only 4.1 nm aluminium oxide, as a comparison.

employed in order to employ identical mirrors, as for the multiple mirror case. Measurement and model are in good agreement.

In order to verify the coordinate frames, to verify the employed Mueller matrices, and to avoid previous on-ground confusion, the authors have rebuilt the SCIAMACHY scanner setup in an optics lab. No new results where found, but all the measurements confirmed all rotations and Mueller matrix signs.

4.3 Diffuser model verification

The assumption that the diffuser acts as a surface diffuser with mirror facets can be checked by changing the angle of the mirror with respect to a fixed light source and a fixed detector. In this case, ϕ_{dif} is fixed as the sum of the incident angle and the outgoing angle, which is the fixed angle between the light source and the instrument. Since $\mathbf{M}_{\mathrm{mir}}$ depends only on the fixed ϕ_{dif}, only the scalar $M_1^{\mathrm{dif}}(\phi_{\mathrm{in}}, \phi_{\mathrm{out}})$ will vary due to the change in the angle of incidence and the outgoing angle (see Eq. 12). This will cause a change in the intensity of the signal, but not in the polarisation properties. Hence, the relative polarisation should remain the same in this situation, irrespective of the angle with respect to the fixed light source and the fixed detector.

A measurement to test this hypothesis has been performed on-ground for SCIAMACHY. A scan over 40° rotation of the
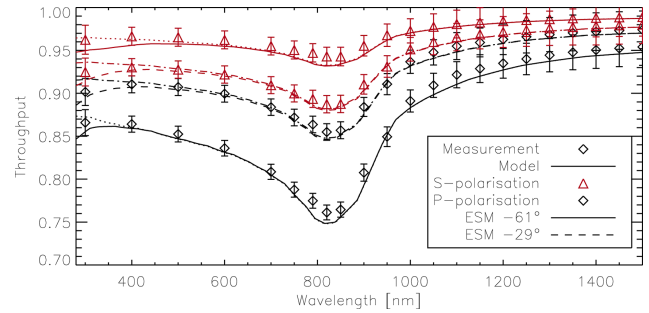

Figure 8. SCIAMACHY scan mirror reflectance for different polarisations (S and P; i.e. $Q = 1$ and $Q = -1$) of the incident light and for different incident angles. Measurements during on-ground calibration are shown as diamonds. The curves represent the reflectance according to the mirror model, using an aluminium mirror with 4.1 nm aluminium oxide and 0.4 nm light oil contamination, under an angle of incidence of either 29° (dashed) or 61° (solid). Dotted and dash–dotted curves indicate the reflectance of clean aluminium instead as a comparison.

mirror was made, while keeping the light source and detector at a fixed position, over which a negligible change in polarisation was observed during the measurements. In Fig. 9, this is shown for a smaller range of rotation angles, near the operational rotation angle of 165°. In the figure, the measured signal of the main science detectors for both s ($Q = 1$) and p polarisation ($Q = -1$) are plotted at 324 nm as a function of the diffuser rotation angle. Both signals are scaled to the maximum of s polarisation for comparison, as the level of the signals is a scanner-independent instrument characteristic, depending on the instrument polarisation sensitivities. The signals show exactly the same response (within the error bars), as shown by their plotted ratio, indicating that the polarisation did not change, only the total reflectance, as expected.

5 Discussion

We present here a method capable of describing the degradation as a function of wavelength, polarisation and scan angle for all Earth-observing instruments employing a (scan) mirror in both low and geostationary orbits. In addition, employing a time-dependent contaminant layer thickness also allows us to describe the degradation as a function of time. Initially this work was started to solve the scan-angle-dependent degradation of SCIAMACHY, but in this paper we have attempted to describe the method in the most generic way, for easy application to other instruments. Not all possible cases have been described, but expansion of the model to for example more mirrors or layers can easily be derived from the presented cases. The model is of interest to all instruments employing (scan) mirrors or other optics suffering from degradation due to contamination. In its current version, the model can be applied to provide detailed scan-angle and wavelength
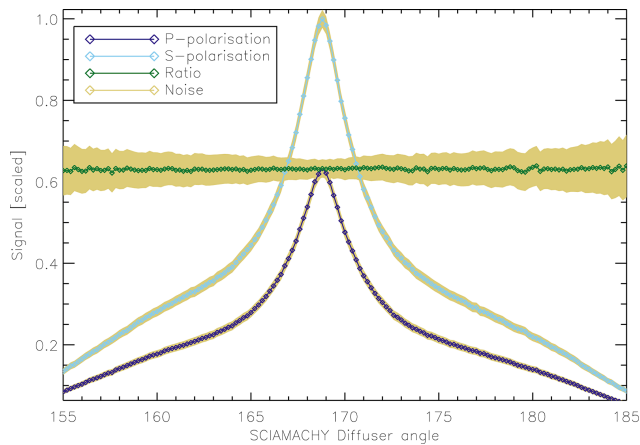
Figure 9. Diffuser model verification: scaled measured SCIA-MACHY signal of the main science detectors as a function of the commanded diffuser angle for both s ($Q = 1$) and p polarisation ($Q = -1$) at 324 nm. Estimated uncertainties or noise (1σ) are indicated by the filled yellow areas. As expected, the ratio between s and p polarisation (green curve) does not change as a function of the diffuser angle.

behaviour as a function of time, allowing for accurate correction, which is needed for precise (trend) analyses. We will further expand on this and illustrate it by the application to SCIAMACHY in-flight measurements in the next paper in this series.

For application to in-flight satellites, several properties must be known: the instrument response to polarisation, the mirror's optical properties (along with its initial contaminations), and the in-flight contaminant optical properties. The model is not wavelength limited, as long as the optical properties of the mirror are known for the wavelength of interest. Issues like a low signal or other instrument limitations will be the limiting factor for the application of the model. The in-flight contaminant optical properties especially are often unknown, and assumptions will have to be made. In the next paper in the series, we will present how this can be done for SCIAMACHY.

We have verified all assumptions and models, and thus removed any remaining sign or frame inconsistencies. All formulae and verification results are fully consistent with each other. In previous measurements for, e.g., SCIAMACHY (Gottwald and Bovensmann, 2011), different mirror configurations were taken as completely different measurements in sometimes conflicting or partially defined polarisation frames. The current model always employs a well-defined frame with a consistent mathematical Mueller approach. All of these frame definitions and approaches have been used consistently for all verification measurements. With this approach, we were able to describe all the measurements available to us. More proof of the correctness of the assumptions or approach employed will follow in a future paper in the series, where we will show the model as also describing time-dependent in-flight measurement behaviour.

6 Conclusions

We have presented a model for accurately describing reflection and polarisation properties of multiple scan mirrors and diffusers in space. This model includes the impact of contamination, both spectrally and scan angle dependent. The model can easily be applied to any satellite, both in low and geostationary orbits, employing (scan) mirrors or other optics suffering from degradation due to contamination. Also, in cases where no scan-angle-dependent degradation is present, but only wavelength-dependent degradation, the model allows for accurate in-flight corrections, provided that information on the contamination can be constrained. Our hypothesis is that both scan mirrors and diffusers suffer from a thin absorbing layer of contaminant, which slowly builds up over time. We described this transmission, polarisation and angle dependence of mirrors, including multi-layers using the Mueller matrix formalism and Fresnel equations. In this paper, we have gone into explicit detail with respect to the handedness of the polarisation and mathematical signs, accompanied by detailed illustrations and descriptions. We resolve the long-standing ambiguities in the application of Mueller matrix and Fresnel calculations in (out-of-plane) reflections. As an application, the SCIAMACHY scanner has been modelled based on this multiple-layer contaminated mirror hypothesis. The model was checked against all known on-ground measurements, and shows excellent agreement under those conditions.

Looking to the future, the current model which will be used in the next paper in this series to investigate the observed UV–VIS signal loss over time and the scan-angle-dependent degradation of SCIAMACHY onboard ENVISAT.

References

Azzam, R. M. and Bashara, N.: Ellipsometry and Polarized Light, Elsevier, 1987.

Barbaro, A., Mazzinghi, P., and Cecchi, G.: Oil UV extinction coefficient measurement using a standard spectrophotometer, Adaptive Optics, 30, 852–857, doi:10.1364/AO.30.000852, 1991.

Born, M. and Wolf, E.: Principles of Optics, with contributions by: Bhatia, A. B., Clemmow, P. C., Gabor, D., Stokes, A. R., Taylor, A. M., Wayman, P. A., and Wilcock, W. L.,

986 pp., ISBN:0521642221, Cambridge, UK, Cambridge University Press, 1999.

Bramstedt, K., Noël, S., Bovensmann, H., Burrows, J., Lerot, C., Tilstra, L., Lichtenberg, G., Dehn, A., and Fehr, T.: SCIA-MACHY Monitoring Factors: Observation and End-to-End Correction of Instrument Performance Degradation, in: Atmospheric Science Conference, Vol. 676 of ESA Special Publication, 2009.

Burge, D. K. and Bennett, H. E.: Effect of a Thin Surface Film on the Ellipsometric Determination of Optical Constants, J. Opt. Soc. Am., 54, 1428–1433, 1964.

Chommeloux, B., Baudin, G., Gourmelon, G., Bezy, J.-L., van Eijk-Olij, C., Schaarsberg, J. G., Werij, H. G., and Zoutman, E.: Spectralon diffusers used as in-flight optical calibration hardware, in: Society of Photo-Optical Instrumentation Engineers (SPIE) Conference Series, edited by Chen, P. T., McClintock, W. E., and Rottman, G. J., Vol. 3427 of Society of Photo-Optical Instrumentation Engineers (SPIE) Conference Series, 382–393, 1998.

Delwart, S.: Instrument Calibration Methods and Results, in: IOCCG Level 1 Workshop, 2010.

Dobber, M.: Ambient scan mirror and on-board diffuser calibration of the SCIAMACHY PFM, issue 1 (TN-SCIA-1000TP/194), Tech. rep., TPD, 1999.

Edlou, S. M., Smajkiewicz, A., and Al-Jumaily, G. A.: Optical properties and environmental stability of oxide coatings deposited by reactive sputtering, Adaptive Optics, 32, 5601–5605, doi:10.1364/AO.32.005601, 1993.

Eplee Jr., R. E., Patt, F. S., Barnes, R. A., and McClain, C. R.: SeaWiFS long-term solar diffuser reflectance and sensor noise analyses, Adaptive Optics, 46, 762–773, doi:10.1364/AO.46.000762, 2007.

Fuqua, P. D., Morgan, B. A., Adams, P. M., and Meshishnek, M. J.: Optical Darkening During Space Environmental Effects Testing – Contaminant Film Analyses, Report TR-2004(8586)-1, Aerospace Corp, El Segundo CA, 2004.

Georgiev, G. T. and Butler, J. J.: Long-term calibration monitoring of Spectralon diffusers BRDF in the air-ultraviolet, Adaptive Optics, 46, 7892–7899, doi:10.1364/AO.46.007892, 2007.

Gottwald, M. and Bovensmann, H.: SCIAMACHY, Exploring the Changing Earth's Atmosphere, DLR, 2011.

Gottwald, M., Krieg, E., Noël, S., Wuttke, M., and Bovensmann, H.: Sciamachy 4 Years in Orbit-Instrument Operations and In-Flight Performance Status, in: Atmospheric Science Conference, Vol. 628 of ESA Special Publication, 2006.

Green, D. B.: Satellite Contamination and Materials Outgassing Knowledgebase – An Interactive Database Reference, NASA STI/Recon Technical Report N, 1, 41072, 2001.

Haynes, W. M. (Ed.): CRC Handbook of Chemistry and Physics, CRC Press/Taylor and Francis, Boca Raton, FL., 93 (internet version), 2013.

Hecht, E.: Optics, 2nd Edn., Adisson-Wesley, 1987.

Jeurgens, L. P. H., Sloof, W. G., Tichelaar, F. D., and Mittemeijer, E. J.: Structure and morphology of aluminium-oxide films formed by thermal oxidation of aluminium, Thin Solid Films, 418, 89–101, 2002.

Joos, F., Buenzli, E., Schmid, H. M., and Thalmann, C.: Reduction of polarimetric data using Mueller calculus applied to Nasmyth instruments, in: "Observatory Operations: Strategies, Processes, and Systems II", edited by: Brissenden, R. J. and Silva, D. R., 70161I–70161I–11, 2008.

Keller, C. U.: Instrumentation for astrophysical spectropolarimetry, in: Astrophysical Spectropolarimetry, edited by: Trujillo-Bueno, J., Moreno-Insertis, F., and Sánchez, F., 303–354, 2002.

Krijger, J. M., Aben, I., and Schrijver, H.: Distinction between clouds and ice/snow covered surfaces in the identification of cloud-free observations using SCIAMACHY PMDs, Atmos. Chem. Phys., 5, 2729–2738, doi:10.5194/acp-5-2729-2005, 2005a.

Krijger, J. M., Tanzi, C. P., Aben, I., and Paul, F.: Validation of GOME polarization measurements by method of limiting atmospheres, J. Geophys. Res.-Atmos., 110, 7305, doi:10.1029/2004JD005184, 2005b.

Lang, R.: GOME-2/Metop-A Level 1B Product Validation Report No. 5: Status at Reprocessing G2RP-R2 v1F, Report EUM/OPS-EPS/REP/09/0619, EUMETSAT, 2012.

Lei, N., Wang, Z., Guenther, B., Xiong, X., and Gleason, J.: Modeling the detector radiometric response gains of the Suomi NPP VIIRS reflective solar bands, in: Society of Photo-Optical Instrumentation Engineers (SPIE) Conference Series, Vol. 8533 of Society of Photo-Optical Instrumentation Engineers (SPIE) Conference Series, doi:10.1117/12.974728, 2012.

McMullin, D. R., Judge, D. L., Hilchenbach, M., Ipavich, F., Bochsler, P., Wurz, P., Burgi, A., Thompson, W. T., and Newmark, J. S.: In-flight Comparisons of Solar EUV Irradiance Measurements Provided by the CELIAS/SEM on SOHO, ISSI Scientific Reports Series, 2, 135, 2002.

Meister, G. and Franz, B. A.: Adjustments to the MODIS Terra radiometric calibration and polarization sensitivity in the 2010 reprocessing, in: Society of Photo-Optical Instrumentation Engineers (SPIE) Conference Series, Vol. 8153 of Society of Photo-Optical Instrumentation Engineers (SPIE) Conference Series, doi:10.1117/12.891787, 2011.

Mott, N. F.: A Theory of the Formation of Protective Oxide Films on Metals, T. Faraday Soc., 35, 1175–1177, 1939.

Noël, S., Bovensmann, H., Skupin, J., Wuttke, M. W., Burrows, J. P., Gottwald, M., and Krieg, E.: The SCIAMACHY calibration/monitoring concept and first results, Adv. Space Res., 32, 2123–2128, doi:10.1016/S0273-1177(03)90532-1, 2003.

Palik, E. D. (Ed.): Handbook of Optical Constants of Solids, Vol. 1, Academic Press, 1985.

Rakic, A. D.: Algorithm for the determination of intrinsic optical constants of metal films: application to aluminum, Adaptive Optics, 34, 4755–4767, doi:10.1364/AO.34.004755, 1995.

Sankarasubramanian, K., Samson, J. P. A., and Venkatakrishnan, P.: Measurement of instrumental polarisation of the Kodaikanal Tunnel Tower Telescope, in: Solar polarization: proceedings of an international workshop held in Bangalore, India, 12–16 October, 1998, edited by: Nagendra, K. N. and Stenflo, J. O., pp. 313–320, Kluwer Academic Publishers, 1999.

Schläppi, B., Altwegg, K., Balsiger, H., Hässig, M., Jäckel, A., Wurz, P., Fiethe, B., Rubin, M., Fuselier, S. A., Berthelier, J. J., De Keyser, J., Rème, H., and Mall, U.: Influence of spacecraft outgassing on the exploration of tenuous atmospheres with in situ mass spectrometry, J. Geophys. Res.-Space, 115, A12313, doi:10.1029/2010JA015734, 2010.

Slijkhuis, S., Aberle, B., and Loyola, D.: Improvements of GDP Level 0 – 1 Processing System in the Framework of CHEOPS-GOME, in: Atmospheric Science Conference, Vol. 628 of ESA Special Publication, 2006.

Snel, R.: In-orbit optical degradation: GOME experience and SCIA-MACHY prediction, in: ERS-ENVISAT Symposium "Looking down to Earth in the New Millennium", CD–ROM, 2000.

Stiegman, A. E., Bruegge, C. J., and Springsteen, A. W.: Ultraviolet stability and contamination analysis of Spectralon diffuse reflectance material, Opt. Eng., 32, 799–804, doi:10.1117/12.132374, 1993.

Thiessen, G. and Broglia, P.: Uber einen Polarisationseffekt an aufgedampften Aluminiumschichten bei senkrechter Lichtinzidenz, Z. Astrophys., 48, p. 81, 1959.

Tilstra, L. G., de Graaf, M., Aben, I., and Stammes, P.: In-flight degradation correction of SCIAMACHY UV reflectances and Absorbing Aerosol Index, J. Geophys. Res.-Atmos., 117, D06209, doi:10.1029/2011JD016957, 2012.

van Harten, G., Snik, F., and Keller, C. U.: Polarization Properties of Real Aluminum Mirrors, I. Influence of the Aluminum Oxide Layer, Publ. Astron. Soc. Pac., 121, 377–383, doi:10.1086/599043, 2009.

van Roermund, F.: SCIAMACHY Cleanliness and Contamination Control Plan, Report PL-SCIA-0000FO/05, BUPS, 1996.

Xiong, X. and Barnes, W.: An overview of MODIS radiometric calibration and characterization, Adv. Atmos. Sci., 23, 69–79, doi:10.1007/s00376-006-0008-3, 2006.

Xiong, X., Chiang, K., Esposito, J., Guenther, B., and Barnes, W.: MODIS on-orbit calibration and characterization, Metrologia, 40, S89, doi:10.1088/0026-1394/40/1/320, 2003.